ACS NANO

www.acsnano.org

ARTICLE

Elucidating Structural Configuration of Lipid Assemblies for mRNA Delivery Systems

Hyunhyuk Tae,[○] Soohyun Park,[○] Li Yang Tan, Chungmo Yang, Yong-An Lee, Younghwan Choe, Torsten Wüstefeld, Sangyong Jung,* and Nam-Joon Cho*

Cite This: https://doi.org/10.1021/acsnano.4c00587

Read Online

ACCESS | Metrics & More | Article Recommendations | Supporting Information

ABSTRACT: The development of mRNA delivery systems utilizing lipid-based assemblies holds immense potential for precise control of gene expression and targeted therapeutic interventions. Despite advancements in lipid-based gene delivery systems, a critical knowledge gap remains in understanding how the biophysical characteristics of lipid assemblies and mRNA complexes influence these systems. Herein, we investigate the biophysical properties of cationic liposomes and their role in shaping mRNA lipoplexes by comparing various fabrication methods. Notably, an innovative fabrication technique called the liposome under cryo-assembly (LUCA) cycle, involving a precisely controlled freeze−thaw−vortex process, produces distinctive onion-like concentric multilamellar structures in cationic DOTAP/DOPE liposomes, in contrast to a conventional extrusion method that yields unilamellar liposomes. The inclusion of short-chain DHPC lipids further modulates the structure of cationic liposomes, transforming them from multilamellar to unilamellar structures during the LUCA cycle. Furthermore, the biophysical and biological evaluations of mRNA lipoplexes unveil that the optimal N/P charge ratio in the lipoplex can vary depending on the structure of initial cationic liposomes. Cryo-EM structural analysis demonstrates that multilamellar cationic liposomes induce two distinct interlamellar spacings in cationic lipoplexes, emphasizing the significant impact of the liposome structures on the final structure of mRNA lipoplexes. Taken together, our results provide an intriguing insight into the relationship between lipid assembly structures and the biophysical characteristics of the resulting lipoplexes. These relationships may open the door for advancing lipid-based mRNA delivery systems through more streamlined manufacturing processes.

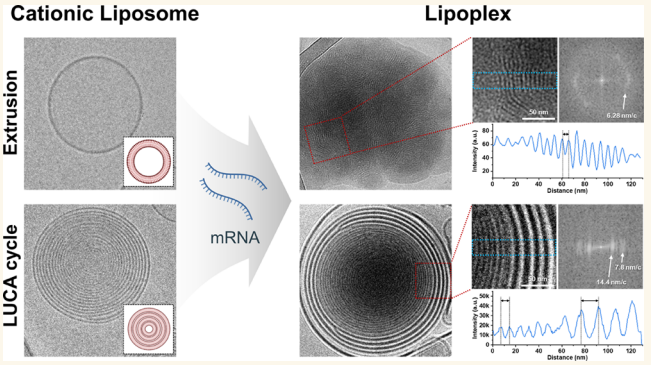

KEYWORDS: *lipid assembly, cationic liposome, multilamellar structure, lipoplex, mRNA delivery, cryo-assembly, biophysics*

INTRODUCTION

The advancement of gene delivery systems employing nucleic acids and carrier molecules offers a promising avenue for addressing a wide range of diseases.[1−3] This approach holds the potential to enable precise control over the expression of disease-related genes, modulate the expression of functional proteins, and coordinate the controlled immune responses.[1−3] In recent years, lipid-based nucleic acid delivery systems have emerged as a cornerstone, facilitating the efficient transport and delivery of genetic materials.[4,5] This prominence is exemplified through the successful deployment of lipid nanoparticles (LNPs) in the development of mRNA vaccines to address coronavirus disease 2019 (COVID-19). This showcases the versatile potential of lipid-based gene delivery systems.[6]

While substantial progress has been achieved in the domain of lipid-based gene delivery systems, research efforts have primarily centered on exploring the use of various lipid formulations.[7−9] Such exploration has encompassed fixed cationic lipids (e.g., 1,2-dioleoyl-3-trimethylammonium-propane (DOTAP)) and multivalent cationic lipids, each with distinct functional effects. Additionally, neutral lipids, such as 1,2-dioleoyl-*sn*-glycero-3-phosphoethanolamine (DOPE), have been incorporated to induce hexagonal phases and promote membrane fusion.[10−12] Furthermore, the inclusion of ionizable lipids has enabled endosomal escape, a critical step in gene delivery, while the integration of advanced lipids into LNPs has advanced organ-specific targeting.[13−15]

Received: January 14, 2024
Revised: March 27, 2024
Accepted: April 4, 2024

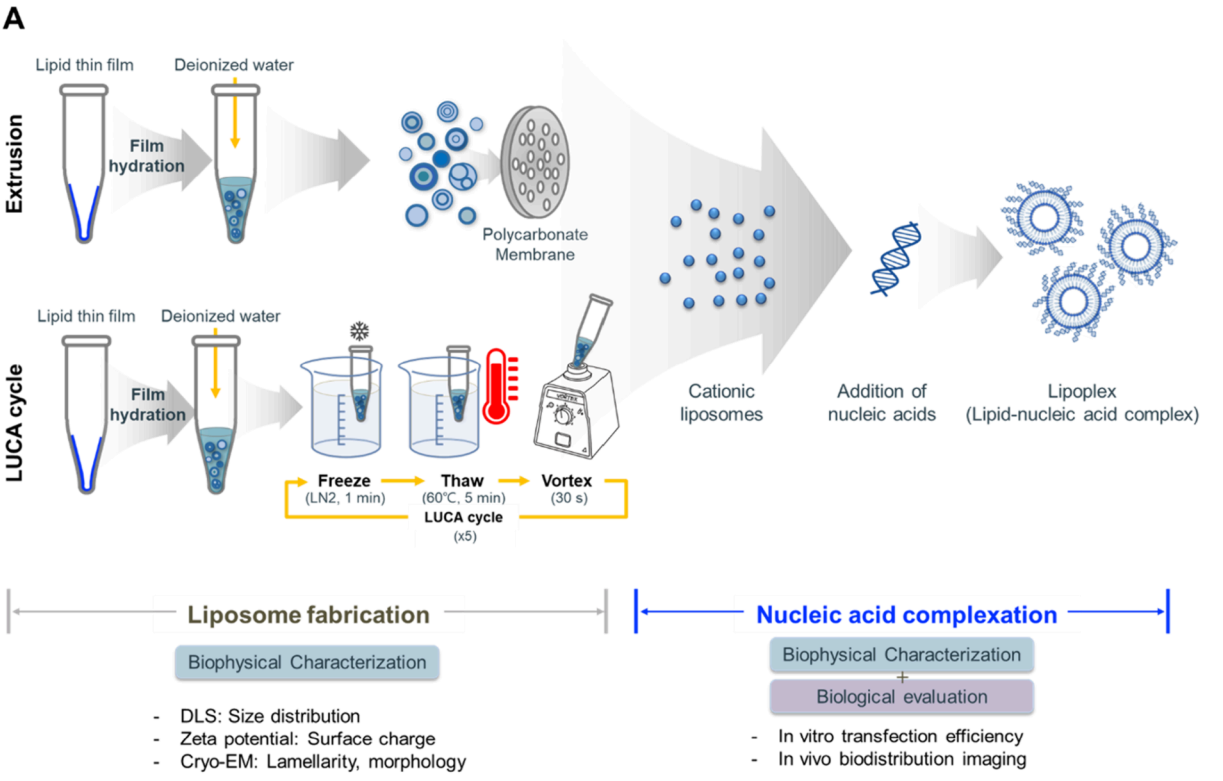

B

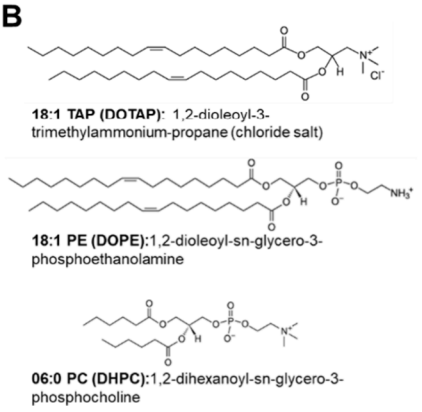

C

Name	Fabrication	Lipid composition (molar ratio)			N/P
		Long-Chain		Short-Chain	
		DOTAP	DOPE	DHPC	
VOR	Vortex	1	1	-	9.0 6.0 3.0 1.5 0.75 0.375
E50	50 nm-extrude	1	1	-	
E400	400 nm-extrude	1	1	-	
LC	LUCA cycle	1	1	-	
L4.0	LUCA cycle, Bicellar mixture (q=4.0)	1	1	0.5	
L2.0	LUCA cycle, Bicellar mixture (q=2.0)	1	1	1	

Figure 1. Experimental framework for investigating the influence of initial liposome characterizations on lipoplex formation. (A) Schematics illustrating the methods for liposome fabrication and nucleic acid complexation, including biophysical and biological assessments. LUCA cycle represents a precisely controlled freeze−thaw-based method utilized in this study, alongside the conventional extrusion method for comparison. (B) Chemical structure of the lipids utilized in this study. DOTAP is a permanently charged monocationic lipid facilitating nucleic acid complexation, DOPE is a neutral helper lipid promoting membrane fusion, and DHPC is a neutral short-chain lipid modulating liposome properties. (C) Table displaying the types of cationic liposomes employed in lipoplex synthesis with different charge ratios (N/P). The N/P denotes the molar ratio of positively charged amine (N = nitrogen) groups to negatively charged nucleic acid phosphate (P) groups. q-ratio denotes the molar ratio of long-chain to short-chain lipids.

On the other hand, a significant knowledge gap remains despite the outstanding progress achieved in lipid-based nucleic acid delivery systems, particularly concerning the influence of biophysical characteristics (e.g., size, lamellarity, morphology, and surface charge) on lipid assemblies and their mRNA complexes.[16] Notably, the biophysical impact on the self-assembly process of these systems is further underscored in the aqueous-phase mixture of cationic liposomes with nucleic acids, termed "lipoplex", due to their inherent flexibility in fabrication derived from various liposome production methods. The resulting assembly features of lipoplex, which are intricately linked to the fabrication methods employed, hold the potential to significantly impact pivotal biological activities.[17,18] However, prior studies have predominantly focused on directly comparing fabrication methods in terms of transfection efficiency,[18−20] thereby making a challenge to decipher whether the functionality of lipoplex depends on specific factors or if certain variables are inconsequential due to the lack of a deeper understanding of the underlying biophysical characteristics. Additionally, the relationship between liposome size and biological activities has produced conflicting results,[21−24] creating ambiguity even in this seemingly straightforward association. Therefore, comprehending the intricate biophysical relationship between cationic lipid assemblies and the attributes of the mRNA lipoplex is of

https://doi.org/10.1021/acsnano.4c00587
ACS Nano XXXX, XXX, XXX−XXX

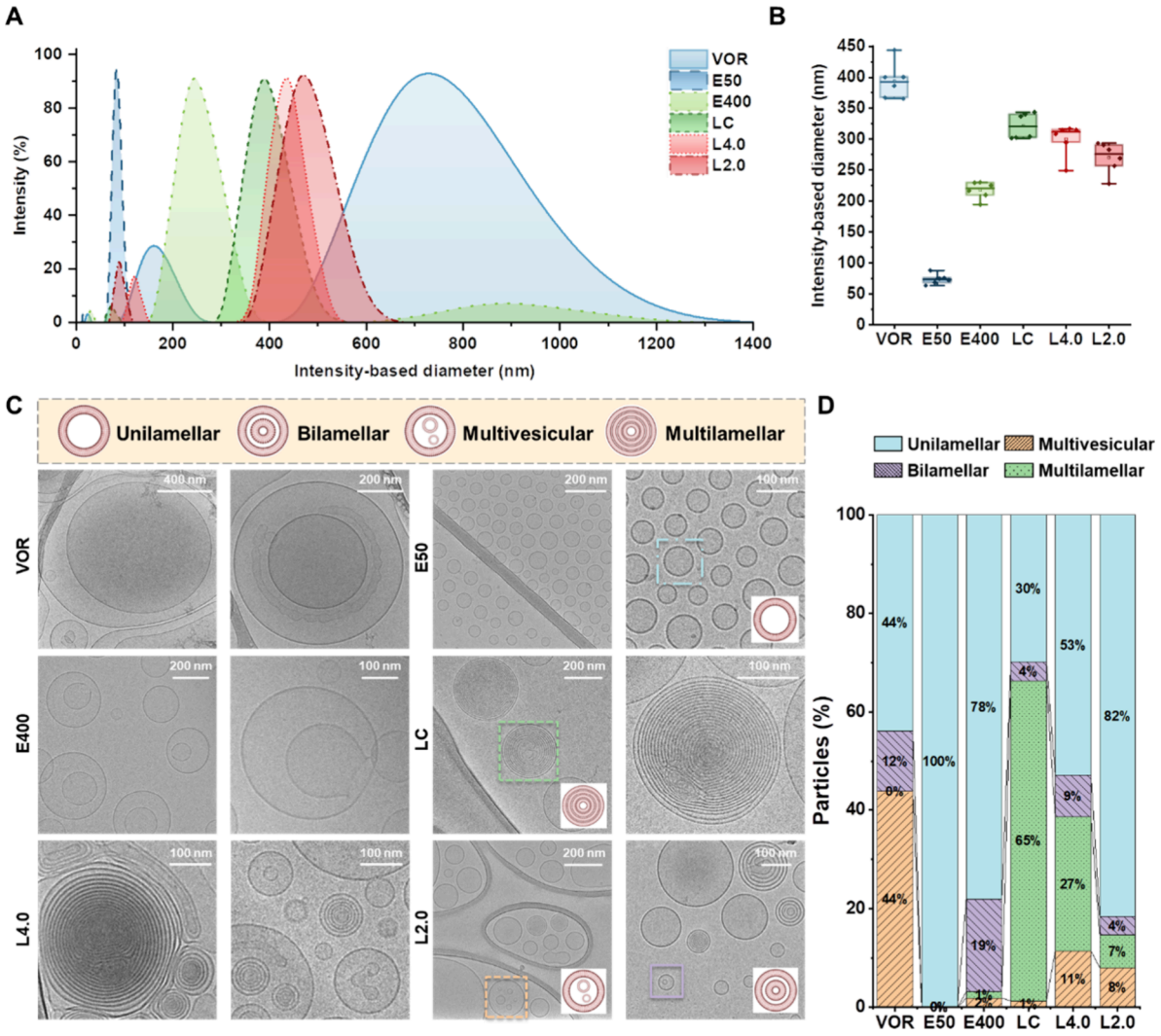

Figure 2. Biophysical characterization of cationic liposomes depending on the fabrication methods and inclusion of short-chain DHPC lipids. (A) Representative size distribution curves obtained from DLS in intensity-weighted mode. (B) Mean diameter measured by DLS after fitting into the correlation function of a single exponential decay (n = 6). (C) Cryo-EM micrographs illustrating structural differences among cationic liposomes. Examples of liposome classification are highlighted in the boxes: blue, unilamellar; green, multilamellar; purple, bilamellar; and orange, multivesicular. The lacey patterns observed in cryo-EM images of E50, LC, and L2.0 were attributed to the underlying copper mesh grid. (D) Qualitative analysis of liposome morphology as determined by cryo-EM (n > 80 for each sample).

paramount importance to fully unlock the therapeutic potential of lipid-based nucleic acid delivery systems.

In this study, we systematically investigated the biophysical characteristics of cationic liposomes and lipoplexes with a particular focus on how different fabrication methods influence the assembly structures of lipids. We began by characterizing cationic liposomes prepared using various fabrication methods with the inclusion of short-chain lipid (1,2-dihexanoyl-*sn*-glycero-3-phosphocholine (DHPC)) in some formulations to tune the lipid assembly. The biophysical factors, such as size distribution, surface charge, lamellarity, and morphology, were examined across liposomes with diverse formulations. Then, we assessed the impact of liposome characteristics on the biophysical properties of mRNA lipoplexes by varying the N/P ratio, which represents the ratio of positively charged cationic lipids to phosphate groups in mRNA. Furthermore, the biological efficacy of these lipoplexes was evaluated to relate the initial liposome structure to lipoplex biophysical characteristics and functionality. Finally, we subjected representative cationic and anionic lipoplexes to a detailed morphological analysis. A comprehensive structural comparison revealed the critical role of the liposome structure and the N/P ratio in shaping the structure of lipoplexes, resulting in distinct structural patterns depending on the self-assembly of liposomes.

RESULTS AND DISCUSSION

Experimental Design. We commenced the examination of cationic liposomes and lipoplexes by employing two different fabrication methods with a focus on unraveling their biophysical properties, as illustrated in Figure 1A. Initially, we opted for the extrusion method, one of the most conventionally employed methods for generating unilamellar liposomes with monodisperse size distribution.[25,26] Despite the time-consuming multistep process, this technique is still widely used due to its exceptional reproducibility, homogeneous size distribution, and its ability to bypass the removal step of organic solvents or detergents.[5,25] Additionally, we introduced a fabrication technique termed the liposome under cryo-

https://doi.org/10.1021/acsnano.4c00587
ACS Nano XXXX, XXX, XXX−XXX

assembly (LUCA) cycle, building upon the freeze−thawing method. Freeze−thawing is another commonly adopted method for homogeneous and unilamellar liposome production, as well as for improving encapsulation efficiency of molecules.[27,28] Through the repetition of this cycle, the ice crystal formation expands the inner liquid phase and fragments the lamellar structure of liposomes, leading to more small and homogeneous populations of lipid self-assemblies.[5,29,30] While the LUCA cycle was originally designed for bicellar mixtures to create supported lipid bilayers (SLBs),[31,32] this approach was extended to produce cationic liposomes and lipoplexes in this study.

For biophysical characterization, we utilized dynamic light scattering (DLS) and zeta potential measurements to analyze the size distribution and surface charge of lipid assemblies, respectively. These parameters are pivotal in understanding the self-assembly dynamics of cationic liposomes with mRNA, where the size and surface charge of the resulting lipoplexes are influenced by the inherent properties of the initial cationic liposomes and the charge ratio between cationic lipids and mRNA.[21,33,34] In addition, cryogenic electron microscopy (cryo-EM) was employed to scrutinize the structural properties of lipid assemblies, including lamellarity and morphology, as their self-assembled structure can exhibit significant variations due to parametric changes such as lipid formulation, fabrication methods, and the mode of complexation.[35−37] For biological evaluation, *in vitro* transfection efficiency of luciferase-encoding mRNA in lipoplexes and *in vivo* biodistribution were measured to elucidate how biophysical characteristics of liposomes and lipoplexes affect the functionality of mRNA lipoplexes.

To fabricate cationic liposomes, DOTAP and DOPE lipids were selected as the foundational lipid composition (Figure 1B), based on their established success in nucleic acid delivery.[38−41] The DOTAP/DOPE system has been studied for decades, suggesting a potential mechanism for nucleic acid delivery wherein membrane fusion is facilitated by the inverted hexagonal phase and reduced bending coefficients of the unsaturated moiety within this complex.[11,24,42] Nevertheless, establishing a direct correlation between these characteristics and biological efficacies remains elusive,[5,43] emphasizing the need for further exploration in DOTAP/DOPE lipoplex systems. Moreover, we added short-chain DHPC lipid to regulate the size and structure of the cationic liposomes. DHPC, commonly used in disc-like bicellar systems with long-chain saturated lipids, disrupts the spherical assembly of liposomes and stabilizes the bilayer disc through edge interactions.[44,45] However, when combined with long-chain unsaturated lipids such as 1,2-dioleoyl-*sn*-glycero-3-phosphocholine (DOPC), DHPC destabilizes the lipid bilayers due to its preference for high curvature, leading to structural modifications including the vesiculation and formation of smaller aggregates.[46−48] Hence, DHPC could serve as a tool to modulate the size distribution and structure of liposomes.

Consequently, six distinct types of cationic liposomes were employed for lipoplex synthesis with different N/P charge ratios (Figure 1C). The vortexed liposome, termed VOR, served as a representation of a large liposome with a broad size distribution and random structures. E50 and E400 represented 50 and 400 nm-extruded liposomes, respectively. E50 was designed to exhibit a unilamellar morphology with a small and uniform size distribution, while E400, although controlled by extrusion, was expected to have a larger size distribution. Likewise, the LUCA cycle was applied to fabricate cationic liposomes, designated as LC. To further modulate the size and structure of LC, short-chain DHPC lipid was subsequently added to the LC formulation. Considering the pivotal role of *q*-ratio in shaping bicellar phases,[45,49] DHPC-incorporated liposomes were fabricated with *q*-ratios of 4.0 and 2.0, denoted as L4.0 and L2.0, respectively.

Biophysical Characterizations of Cationic Liposomes.

Size Distribution. The size distribution of liposomes was first analyzed by the DLS technique. Upon hydration after thin-film formation, VOR exhibited broad size distributions with two distinct multimodal peaks, spanning approximately 180 and 760 nm (Figure 2A). The average diameter of VOR from multiple samples was measured at 393.9 ± 28.9 nm, with a corresponding polydispersity index (PDI) of 0.34, reflecting their less reproducible and heterogeneous nature (Figure 2B, Table S1). This outcome aligns with expectations that the hydration of dried phospholipids in aqueous medium results in the uncontrolled self-assembly of heterogeneous bi- and/or multilamellar liposomes with broad size distribution.[50]

Subsequent extrusion through a 50-nm filter led to the formation of E50, characterized by an extremely narrow size distribution with an average diameter of 73.7 ± 8.3 nm and a PDI of 0.13. Notably, E50 exhibited a singular narrow peak in the multimodal analysis, emphasizing its uniformity. On the other hand, E400 showed a relatively broader size distribution with double multimodal peaks compared to E50, potentially attributed to a larger pore size yielding a certain extent of heterogeneity. Nevertheless, E400 demonstrated a smaller and more uniform size distribution than VOR, hinting at the potential advantages of the extrusion technique in generating liposomes with consistent characteristics.

When the LUCA cycle was introduced, the average diameter of LC was 321.6 ± 20.6 nm, a size falling between those of VOR and E400, with a surprisingly low PDI of 0.20. This implies that the LUCA cycle effectively reduced both the size and size distribution of liposomes, possibly achieved through the freeze−thaw mechanism, causing the fragmentation of lipids by the ice crystals during freezing and subsequent rupture of lipid membrane.[27,29] Intriguingly, the addition of short-chain DHPC lipid led to a slight reduction in liposome size along with a broadening of the size distribution in L4.0. This effect became even more pronounced when the concentration of DHPC was doubled in L2.0. Such observations are likely due to the disordering of the lipid membrane induced by the difference in chain length between long-chain and short-chain lipids,[47,48] ultimately resulting in the formulation of stable liposomes characterized by reduced size alongside an increase in distribution.

As the size distribution of liposomes stands as a crucial factor in the field of pharmaceutical development, the monodisperse size distribution observed in LC represents a significant advantage, rendering the LUCA cycle as a promising method for formulating a lipid-based delivery system. Moreover, this technique offers potential benefits for large-scale production owing to its streamlined process with minimal sample preparation,[32,51] avoiding the use of organic solvents and complex equipment. The LUCA cycle's simplicity makes it a compelling candidate for industrial-scale applications, although comprehensive investigations are warranted to fully explore its potential.

Morphology. We next characterized the morphology of the cationic liposomes by cryo-EM (Figure 2C). VOR displayed

https://doi.org/10.1021/acsnano.4c00587
ACS Nano XXXX, XXX, XXX−XXX

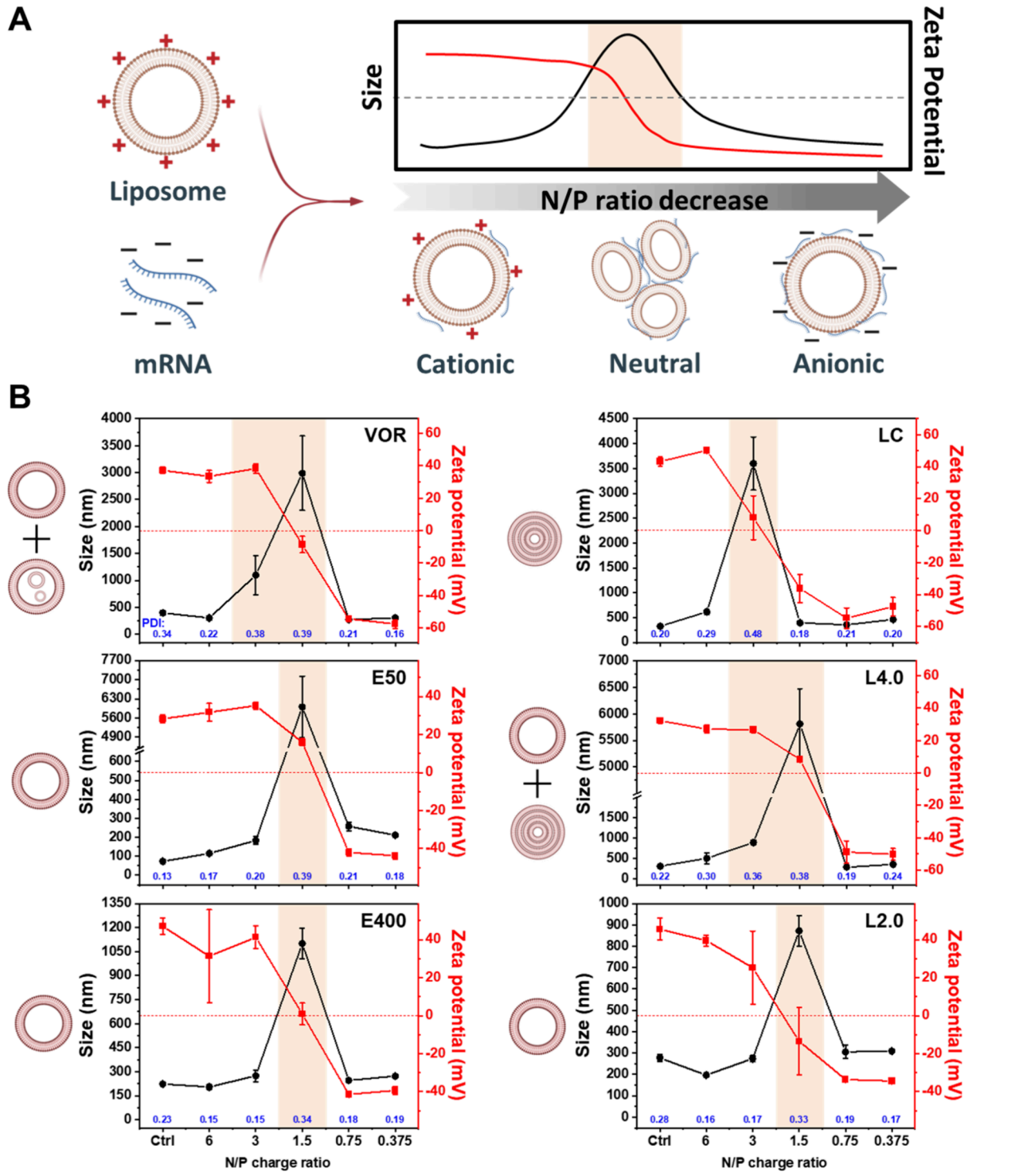

Figure 3. Biophysical property characterization and modulation of lipoplexes to achieve stable and efficient lipoplex formation by tuning the N/P charge ratio of respective cationic liposomes. (A) Schematic representation to show the influence of the N/P charge ratio on the colloidal stability of lipoplexes, which can be inferred from their particle size (black line) and net surface charge (red line). (B) DLS and zeta potential of lipoplexes to assess the size distribution, surface charge, and colloidal stability. The illustrations show the representative structural features present in each cationic liposome formulation. Note that the shaded regions in the graphs indicate the N/P charge ratios associated with unstable lipoplex formation. All data were presented as the mean ± standard deviation (n = 3).

heterogeneous sizes and morphologies, with some liposomes exhibiting elongated vesicular shapes encapsulated within larger liposomes. Quantitative analysis revealed that VOR was predominantly composed of both unilamellar and multivesicular structures, with both types representing 44% of the population (Figure 2D). This heterogeneity closely matched the results obtained from the DLS analysis. On the other hand, extruded liposomes showed a distinct trend of lamellarity compared to the VOR. E50 was entirely composed of unilamellar structures, illustrating that extended extrusion resulted in the rupture of multilamellar structures and the generation of small, uniform unilamellar liposomes. In contrast,

https://doi.org/10.1021/acsnano.4c00587
ACS Nano XXXX, XXX, XXX−XXX

E400 primarily exhibited unilamellar structures accompanied by 19% of bilamellar structures.

LC displayed a distinctive "onion-like" concentric multilamellar morphology, which was unexpected as freeze−thaw methods normally reduce the lamellarity, resulting in unilamellar structure.[28−30] Approximately 65% of LC exhibited multilamellar structures, suggesting that LUCA cycles tend to yield relative homogeneity in size distribution but favor the formation of multilamellar structures over unilamellar structures in DOTAP/DOPE cationic liposomes. This densely packed and highly organized concentric multilamellar structure had previously been observed in liposomes, typically requiring the presence of a cosurfactant with shear stress and/or a high concentration of salt.[52−55] It is noteworthy that unlike conventional multilamellar vesicles, which show poor size homogeneity with diameters exceeding 500 nm,[56,57] the production of monodisperse cationic liposomes featuring such a compact multilamellar structure had not been reported in conventional liposomal systems, especially in the absence of salts. While LNPs with diverse structural configurations, such as solid lipid nanoparticles, nanostructured lipid carriers, and cubosomes, have been developed through modification of lipid compositions and/or the addition of stabilizers,[57] this multilamellar liposome was fabricated without altering existing lipid compositions, presenting the adaptability of the LUCA cycle within conventional cationic liposomal systems. Considering that the system consisted solely of cationic and neutral lipids with similar chain lengths in pure water, it is plausible that the interplay between strong electrostatic charge effects and external forces induced by repetitive phase transitions played a role during this unusual assembly, although further investigation is required for a comprehensive understanding of this phenomenon.

Upon the inclusion of short-chain phospholipid, DHPC, the morphological trajectory revealed a reduction of the onion-like multilamellar structures. This reduction became more prominent as the DHPC concentration increased, particularly when transitioning from L4.0 to L2.0. For instance, upon the addition of DHPC at the same molar ratio as DOPE (L2.0), the proportion of multilamellar liposomes decreased by around a factor of 10, from 65 to 7%, while unilamellar liposomes increased up to 3-fold, from 30 to 82%, in comparison to the case without DHPC (LC). Consistent with the DLS results, L4.0 and L2.0 exhibited more heterogeneous sizes and morphologies, including the presence of elongated shapes and multivesicular structures. This change of morphology in stably formed liposome appears to be attributed to the inclusion of short-chain DHPC, which can lead to membrane destabilization.[48,58] This observation potentially explains the observed decrease in lamellarity during the LUCA cycle. Upon the addition of DHPC at a ratio four times that of DOPE (L0.5) numerous mixed micelles appeared, coexisting with unilamellar and multivesicular liposomes due to the high concentrations of short-chain lipids (Figure S1). Based on these findings, L4.0 and L2.0 were selected for comparative analysis with LC to further understand the formation of lipoplexes and examine how the initial structures of the liposomes influence this process.

In addition, the generalized fluorescence polarization (GP) of Laurdan incorporated into cationic liposomes was measured at excitation wavelengths of 340 nm (GP_{340}) to investigate the lipid packing and hydration status of membranes. Laurdan, renowned for its high sensitivity to the presence and mobility of dipoles, serves as an indicator of the surrounding water molecules' extent and thus provides insights into the dehydration level and degree of lipid packing.[59] A higher GP value indicates a closer lipid packing with lower hydration level on the surface of liposome.[60,61] It was observed that all cationic DOTAP/DOPE liposomes exhibited elevated GP_{340} values compared to the DOPC liposome, attributed to the naturally lower hydration level in DOPE-enriched lipid membranes relative to lamellar PC lipid membranes[62] (Figure S2). Furthermore, the higher GP_{340} value in small E50 compared to E400 is possibly due to the closer packing and reduced hydration of PE lipids in increased membrane curvature.[63] Notably, multilamellar LC exhibited a higher GP_{340} value than unilamellar E400, demonstrating a lower hydration level and tighter packing of lipid membranes in the multilamellar structure. Further reduction in hydration was observed in DHPC-embedded L4.0 and L2.0, which might be attributed to the rigid nature of DHPC resulting from saturated carbon chains.[64] Collectively, these findings suggest that the lipid membranes of multilamellar LC are more tightly packed and less hydrated compared to the unilamellar structure in E400.

Biophysical Characteristics of mRNA Lipoplexes. Next, we systematically formulated lipoplexes by varying the molar ratio between the cationic lipid and mRNA to achieve stable and efficient lipoplex formation. Here, the N/P ratio represents the molar ratio of DOTAP (positively charged amine group N) to phosphate groups in mRNA (negatively charged phosphate group, P). During the complexation of cationic liposomes with nucleic acids, the liposomes initially bind to nucleic acids molecules, and aggregation begins when zeta potentials of lipoplexes approach to zero (Figure 3A).[33,65] The colloidally unstable regime is typically observed around a neutral surface charge, leading to the potential aggregation of lipoplexes. With an excess of either negative or positive charge, a colloidally stable lipoplex can be formulated with discrete particle sizes by repulsive electrostatic forces. As N/P ratio serves as a key parameter for the colloidal stability, particle characteristics, and the targeting selectivity,[5,41] it is imperative to investigate the effect of N/P ratio to optimize the lipoplex formulation.

Generally, higher charge ratios (N/P > 6) resulted in predominantly positive-charged particles, while lower charge ratios (N/P < 1.0) produced negative-charged lipoplexes. Notably, the majority of lipoplexes exhibited a near-neutral surface charge and reached their largest size at an N/P ratio of 1.5, where nearly equivalent molar ratio of cationic lipids and nucleic acids coexisted. However, an exception was found with LC-based lipoplexes, which achieved their largest size at a N/P ratio of 3.0 (Figure 3B). This peculiar observation in LC-based lipoplexes can be elucidated by the significantly high proportion (~65%) of multilamellar structures resulting from the freeze−thaw cycles. As fewer nucleic acids were required to neutralize the overall charge when fewer cationic lipids were exposed on the surface, a higher N/P ratio was necessary to achieve near-neutral zeta potential. Similarly, relatively larger lipoplexes (~1000 nm) were formed at an N/P ratio of 3.0 in the cases of VOR and L4.0. This occurrence can be attributed to their comparatively lower proportion of uni/bilamellar structures. Interestingly, lipoplexes derived from E50 with an N/P ratio of 1.5 (E50-1.5) formed notably larger aggregates than their E400 counterparts (E400-1.5). This result could be ascribed to the substantially larger surface area of E50, stemming from its 100% unilamellar structure with a smaller

https://doi.org/10.1021/acsnano.4c00587
ACS Nano XXXX, XXX, XXX−XXX

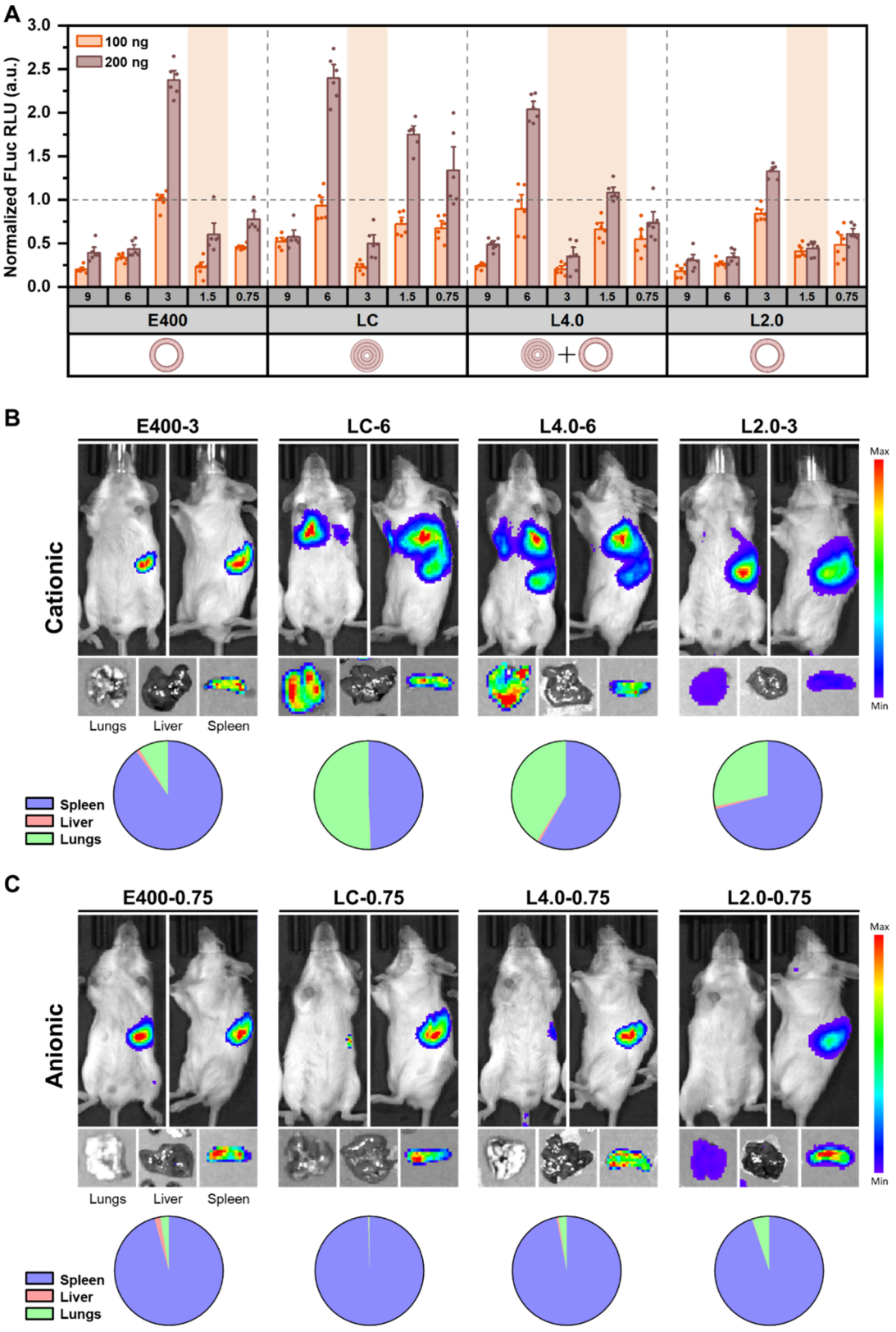

Figure 4. *In vitro* transfection efficiency and *in vivo* biological efficacy of lipoplexes at varied N/P charge ratios of respective cationic liposomes. (A) Relative luciferase expression in HEK293T cells after 24 h of treatment with mRNA lipoplexes (100 and 200 ng mRNA/well, n = 6). The highlighted orange regions in the graphs represent the N/P charge ratios associated with unstable lipoplex formation, as determined via biophysical analysis, as shown in Figure 3. A horizontal dashed line represents the expression level of E400-3 with 100 ng set to 1.0 arbitrary units (a.u.). All data were presented as the mean ± standard deviation (S.D.). Bioluminescence imaging of BALB/c mice after intravenous (IV) administration of (B) cationic and (C) anionic lipoplexes formulated by different liposomes with various charge ratios. Pie charts show the relative contribution of each organ to the total signal.

https://doi.org/10.1021/acsnano.4c00587
ACS Nano XXXX, XXX, XXX−XXX

diameter of approximately 70 nm, which differs from the other liposome configurations. As the surface charge of lipoplexes shifts from neutral to negative (at smaller N/P ratios), the complexes exhibited enhanced stability and a reduced size, attributed to an excess of mRNA counteracting the positive charge of DOTAP in cationic liposomes. These trends in size and zeta potential changes were consistent among all lipoplexes. In particular, liposomes with multilamellar or multivesicular structures tended to aggregate at relatively high N/P ratios in comparison to their uni/bilamellar liposomes. This behavior is likely due to the limited exposure of cationic lipids on the surface of multilamellar or multivesicular liposomes. Collectively, these findings demonstrate that the region of colloidal instability in lipoplexes is significantly influenced by both initial liposome morphology and the N/P ratios.

GP_{340} values of E400 and LC-based lipoplexes were further assessed by varying N/P ratios to investigate the impact of liposome structures on the hydration within lipoplex (Figure S3). The effect of mRNA on GP_{340} for lipoplexes is described as ΔGP_{340} = GP_{340} of lipoplexes − GP_{340} of liposomes. While both E400 and LC-based lipoplexes displayed a consistent trend of increasing GP_{340} with decreasing N/P ratios,[62] it is noteworthy that LC-based lipoplexes tended to exhibit lower ΔGP_{340} values compared to E400-based lipoplexes. As dehydration in lipoplex requires a tight contact between nucleic acids and cationic lipids,[38,66] the observed lower ΔGP_{340} values in LC-based lipoplexes suggest a large hydration and relatively loose association of mRNA molecules upon complexation with multilamellar LC. This phenomenon is also likely attributable to the denser lipid packing and lower hydration level of multilamellar membranes in LC relative to the unilamellar E400, making them more resistant to the membrane remodeling by complexation with mRNA.

Biological Efficacy of mRNA Lipoplexes. To evaluate the biological efficacy of lipoplexes, *in vitro* cellular transfection experiments were conducted using HEK293T cells. Following a 24 h treatment with lipoplexes, the cells were lysed to measure the relative intensity of luciferase expression. A prevailing trend revealed that lipoplexes with aggregated particles, such as lipoplexes derived from E400 with an N/P ratio of 1.5 (E400-1.5) and from LC with an N/P ratio of 3 (LC-3), consistently yielded lower transfection efficiency (Figure 4A). Conversely, those in the vicinity of the aggregation threshold, such as positively charged adjacent lipoplexes (e.g., E400-3 and LC-6), consistently demonstrated higher efficiency. However, excessively high N/P ratios (~9.0) resulted in reduced transfection efficiency for all lipoplexes, likely due to increased cytotoxicity stemming from an excess of cationic lipids and/or the inefficient release of mRNA.[5,67] An interesting pattern was observed within the N/P ratio range of approximately 3.0−6.0, which was dependent on the initial liposome structures. For instance, L4.0-based lipoplexes, composed of a lower proportion of uni/bilamellar liposomes, exhibited the highest luciferase expression at an N/P ratio of 6.0 and the lowest values at an N/P ratio of 3.0. In contrast, L2.0-based lipoplexes displayed a transfection efficiency trend akin to that of E400-based ones, aligned with their high contents of unilamellar structures similar to those of E400. Notably, negatively charged LC-based lipoplexes (e.g., LC-1.5 and LC-0.75) exhibited luciferase expression levels comparable to those of cationic lipoplexes such as E400-3 and LC-6, deviating from observations in other types of lipoplexes.

VOR-based lipoplexes displayed significant deviations in luciferase expression levels without a discernible trend (Figure S4). These deviations are probably attributed to variations in complex formation arising from the heterogeneity of vortexed liposomes. Meanwhile, lipoplexes derived from E50 demonstrated low luciferase expression across all N/P ratios. While it is essential to approach the size effects of lipoplex with caution,[5,68] the low transfection efficiency in E50-derived lipoplexes could potentially be linked to the small size of lipid assemblies.[10,21] This hypothesis is supported by the notable difference in performance observed between E400-derived lipoplexes and E50-derived lipoplexes. Despite sharing a similar liposome morphology achieved through extrusion, the E400-based lipoplexes derived from large liposomes displayed a transfection efficiency higher than that of their E50-derived counterparts at the same N/P ratios. This emphasizes the importance of the lipid assembly size in transfection outcomes by lipoplexes, particularly in cases derived from extruded liposomes.

While neutral LNPs primarily target the liver,[69] it has been reported that lipoplexes can target specific organs by simply tuning the N/P charge ratio.[5,40] Cationic lipoplexes have demonstrated the ability to target the lung or both the lung and the spleen, whereas anionic lipoplexes exhibit specific targeting of the spleen. This phenomenon has led to the development of vaccines that target dendritic cells in the spleen.[40] Additionally, similar surface charge-dependent selective organ targeting (SORT) LNPs have been designed by incorporating charged lipids into conventional LNPs.[15] Against this backdrop, we evaluated the *in vivo* biological efficacy and organ-selective biodistribution of both cationic and anionic lipoplexes, focusing on extruded and LUCA-cycled lipoplexes, which displayed low cytotoxicity and effective *in vitro* transfection with distinct structural discrepancies, as well as consistent colloidal stability for 1 week when stored at 4 °C (Figures S5 and S6).

As shown in Figure 4B, the cationic lipoplex E400-3, derived from E400 with an N/P ratio of 3, primarily expressed luciferase in the spleen, consistent with a previous outcome observed at the same charge ratio.[40] E400-6, possessing a higher positive charge, displayed an enhanced targeting to the lung alongside the spleen, indicating that an elevation in the N/P ratio can increase lung targeting (Figure S7). Notably, this targeting pattern persisted in lipoplexes derived from LC, as evidenced by the targeting of both the lung and spleen by cationic LC-6. On the other hand, anionic E400-0.75 and LC-0.75 demonstrated clear spleen-specific targeting ability (Figure 4C). The consistent trend in organ-targeting ability was observed even after the inclusion of the short-chain DHPC lipid, demonstrating the organ-targeting biological efficacy of lipoplexes with diverse structural properties.

It should be highlighted that the *in vivo* organ-targeting abilities of lipoplexes are significantly influenced by their N/P ratios, whereas the N/P ratios for optimal *in vitro* transfection efficiency are intricately governed by the initial liposome morphology. Taken together, these findings suggest variability in the optimal N/P ratio in lipoplexes, contingent upon the structural characteristics of cationic liposomes, thereby exerting a profound impact on biological efficacy. Beyond the influence of lipid compositions, this emphasizes the importance of simultaneously considering both the cationic liposome structure and N/P ratio when designing mRNA delivery systems.

https://doi.org/10.1021/acsnano.4c00587
ACS Nano XXXX, XXX, XXX−XXX

Given the critical role of nanostructural properties in governing the functionality of lipid-based delivery systems,[57] it is further anticipated that multilamellar structure observed in LC will have a significantly influence on the detailed biological traits of these systems, as multilamellar configuration may impact various aspects, including the interaction between cationic lipids and cell membranes, the loading and release capacity of drug/nucleic acids, and the efficiency of gene transfections of nucleic acids under specific conditions.[57,70−72] In addition, the multilamellar structure in these systems can influence immunogenicity.[73] For example, it was observed that large multilamellar aggregates of archaeosomes exhibited superior immunogenicity compared to their unilamellar counterparts in a comparative study.[74] This finding suggests that the specific structural organization of multilamellar aggregates might confer enhanced immunogenic properties, underscoring the necessity for future investigations to identify the complex relationship between multilamellar nanostructure and the biological characteristics of lipid-based delivery systems.

Structural Characteristics of Cationic and Anionic Lipoplexes. To further understand how the structure of the lipid assembly affects the structure of lipoplexes, we next conducted cryo-EM imaging experiments. Cationic and anionic lipoplexes were selected based on their net charge and biological efficacy, focusing on the N/P ratios near the aggregation points. For lipoplexes prepared from E50, E400, and L2.0, the neutral charge point was identified at a N/P = 1.5. Consequently, cationic and anionic lipoplexes were studied at N/P ratios of 3 and 0.75, respectively. On the other hand, lipoplexes derived from VOR, LC, and L4.0 displayed relative instability within the N/P range of 3−1.5. Therefore, for these lipoplexes, we selected cationic and anionic cases at N/P ratios of 6 and 0.75. It is noteworthy that the initial liposome structure of the latter cases displayed a relatively low content of uni/bilamellar structures compared to the former cases. Representative cryo-EM images are presented in Figure 5.

In cationic lipoplexes (Figure 5A), high-contrast thickened layers with voids were observed in VOR-6, indicating a condensed complex structure formed by the interaction between nucleic acids and cationic lipids within the lipoplex.[75,76] This structural feature appeared to be influenced by a high fraction (44%) of multivesicular structures in VOR, as smaller mRNA molecules might not exert a significant impact on the structure of much larger and more flexible initial liposome structure of VOR. When anionic VOR-0.75 was formulated with excess mRNA (Figure 5B), it led to the formation of paired lamellar structures within and between lipoplex particles, although hollow space was observed within lipoplex due to the large and multivesular liposome structure of VOR. This sandwich-like lamellar phase created a characteristic 'fingerprint' pattern, a feature often observed in DOTAP/DOPE lipoplex systems, arising from strong electrostatic interactions between the cationic lipid membrane and anionic mRNA molecules.[11]

In contrast, E50-derived lipoplexes displayed compact lamellar structures with a denser interior when complexed with either small (E50-3) or large (E50-0.75) amounts of mRNA. Moreover, E50-3 exhibited interconnected and elongated structures compared to other cationic lipoplexes, likely influenced by the high curvature and surface area of E50 and partially accounting for the low transfection efficiency observed in E50-3.[77] Similarly, E400-3 displayed a series of

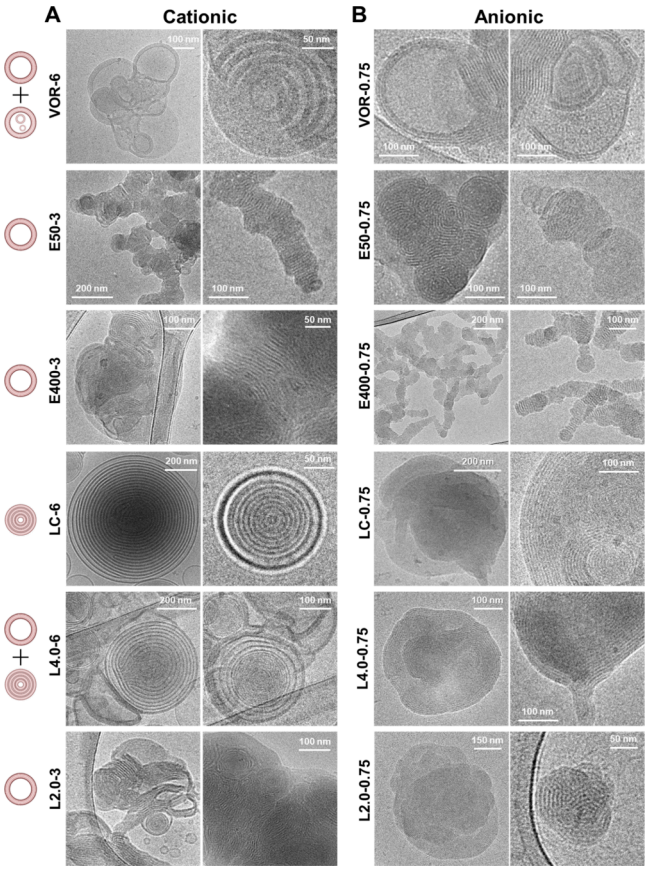

Figure 5. Representative cryo-EM micrographs of (A) cationic and (B) anionic lipoplexes selected based on net charges and in vitro transfection efficiency. The illustrations on the left show representative structural features of the initial cationic liposomes for each lipoplex. Variations in perceived resolution are attributed to differences in magnification arising from various sizes of lipoplexes.

packed lamellar structures, representing the 'fingerprint' pattern of lipoplex. This lipoplex exhibited a larger size with a relatively spherical shape compared to that of E50-3, leading to higher transfection efficiency. On the contrary, E400-0.75 exhibited elongated structures linked by short-length multilamellar complexes, likely due to the strong electrostatic interactions by mRNA and the susceptibility of E400 to shape change compared to smaller E50.[78,79] These elongated structures are consistent with observations in previous studies, where excess nucleic acids resulted in spaghetti-like tubular protrusions or extended periodical multilamellar structures in low N/P ratio conditions.[77,78] Therefore, the elongated structures of E400-0.75 appear to be induced by excess mRNA amounts, partly contributing to the reduced transfection efficiency in vitro.

Strikingly, the concentric multilamellar structure in LC was preserved in cationic LC-6 even after mRNA incorporation. The outer layers of LC-6 increased in thickness compared to LC, while the inner layers transformed into densely packed states as a result of the binding of mRNA. This preservation of the liposome structure in the lipoplex was solely observed in cases characterized by highly packed concentric multilamellar structures in LC. This behavior stands in stark contrast to conventional unilamellar liposomes such as E50 and E400, which tend to undergo a transformation into twisted intricate

https://doi.org/10.1021/acsnano.4c00587
ACS Nano XXXX, XXX, XXX−XXX

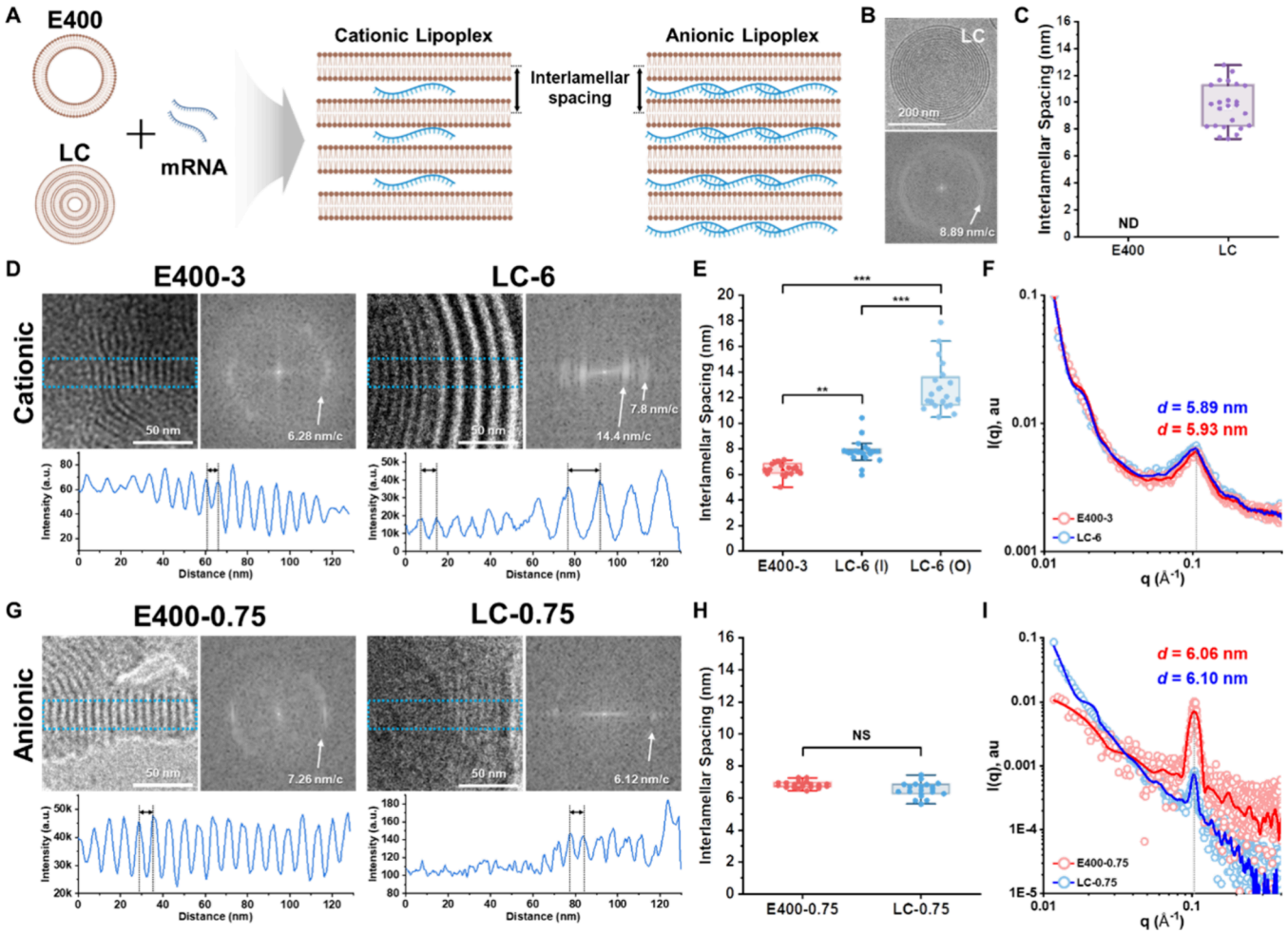

Figure 6. Comparison of self-assembly structures of E400 and LC-based lipoplexes. (A) Schematic representations of unilamellar E400 and multilamellar LC with the ordered structure of the corresponding cationic and anionic lipoplexes highlighting interlamellar spacing. (B) Representative cryo-EM and FFT images of LC revealing a frequency of 8.89 nm/c (bilayer repeat). (C) Interlamellar spacings of E400 and LC analyzed using the pixel intensity profile from cryo-EM images (n > 20 for each sample, mean ± S.D.). (D) Representative cryo-EM images of cationic lipoplexes highlighting the ordered structure and corresponding FFT images and pixel intensity profile to analyze the repeat distances. (E) Interlamellar spacing of cationic lipoplexes analyzed from cryo-EM images (n > 20 for each sample). I and O denote the inner and outer parts of LC-6, respectively. (F) SAXS profiles for cationic lipoplexes with d-spacing calculated from the peak position. (G) Representative cryo-EM images of anionic lipoplexes highlighting the ordered structure and corresponding FFT images and pixel intensity profile to analyze the repeat distances. (H) Interlamellar spacing of anionic lipoplexes analyzed from cryo-EM images (n > 20 for each sample). (I) SAXS profiles for anionic lipoplexes with d-spacing were calculated from the peak position. Data are reported as the mean ± standard deviation and P values of <0.05 were considered statistically significant (*p < 0.05, **p < 0.01, and ***p < 0.001).

assemblies upon nucleic acid complexation. On the other hand, anionic LC-0.75 exhibited conventional lamellar structures by the addition of mRNA, suggesting that strong electrostatic interactions induced by excess mRNA remodeled the concentric multilamellar structures into the fingerprint pattern. Upon adding short-chain DHPC, L4.0−6 displayed a hybrid structure featuring both concentric multilamellar and thickened layers, likely induced by the mixed multilamellar, uni/bilamellar, and multivesicular morphologies of L4.0. As the DHPC content increased, L2.0−3 exhibited fingerprint-like multilamellar structures similar to E400−3, primarily due to its higher porportion of unilamellar structures. In anionic lipoplexes, both L4.0−0.75 and L2.0−0.75 displayed typical closely packed fingerprint patterns when exposed to excess mRNA.

To conclude, our findings underscore that both the structure of the cationic liposome and the N/P ratio exert a significant influence on the structure of mRNA lipoplex, even when the lipid composition remains the same. This highlights the significance of the manufacturing process in modulating the structure of cationic lipid assemblies and the potential for manufacturing process development to modulate the structure of lipid-based assemblies and enhance mRNA delivery systems.

Structural Comparison in Extruded and LUCA-Cycled Liposomes and Lipoplexes. In order to gain a deeper understanding of the morphological structure of lipid assemblies, we conducted a comparative analysis of the detailed repeat distances within lamellar layers of the cationic/anionic representative lipoplexes from 400 nm-extruded E400 and LUCA-cycled LC (Figure 6A). Prior to mRNA complexation, the cryo-EM and fast Fourier transform (FFT) images of LC revealed a lamellar pattern arising from an onion-like concentric multilamellar structure, with the interlamellar spacing of 9.68 ± 1.61 nm (Figure 6B,C). To further analyze the repeat distances of lamellar layers in lipoplexes, featured lamellar structures were selected from the original

https://doi.org/10.1021/acsnano.4c00587
ACS Nano XXXX, XXX, XXX−XXX

cryo-EM images followed by FFT and pixel intensity profile analysis (Figure S8).

Upon complexation with mRNA, the cationic E400-3 showed a single lateral repeat of lamellar structure with periodic layers of electron density, clearly observed by FFT image analysis and intensity line profiling, while the cationic LC-6 notably exhibited two divided interlamellar spacings (the sum of the thickness of the lipid bilayer and the water layer containing mRNA) with major frequencies of 7.8 and 14.4 nm/c, as supported by line plot of the same area (Figure 6D). The average interlamellar spacing of E400-3 was 6.60 ± 1.16 nm, which was smaller than those observed in LC-6; the outer lamellar layers exhibited a spacing of 12.74 ± 1.98 nm, while the inner lamellar layers were packed with a spacing of 7.83 ± 0.93 nm (Figure 6E). The distinct interlamellar spacing in LC-6 suggests that mRNA might be differently encapsulated and/or packed in inner or outer parts. The lamellar structures within cationic lipoplexes were also confirmed through small-angle X-ray scattering (SAXS) analysis (Figure 6F), although E400-3 and LC-6 showed similar *d*-spacing. This discrepancy in observations can be ascribed to variations in the sensitivity of techniques, where SAXS characterizes large-scale bulk analysis and cryo-EM provides the localized morphology with a focus on individual particles.[80,81] Therefore, these measurements possess the capacity to synergistically contribute to the comprehensive analysis of lipoplex structures.[82] When excess mRNA was incorporated, both E400−0.75 and LC-0.75 revealed the characteristic lamellar pattern of diffraction spots with single frequencies in FFT analysis, with similar interlamellar spacings of 6.99 ± 0.31 and 6.51 ± 0.45 nm, respectively (Figure 6G,H). These findings were further corroborated by SAXS analysis (Figure 6I). Taken together, the observed interlamellar spacings were consistent with values reported for multilamellar structures in lipoplex,[83,84] indicating that excess mRNA remodeled lipoplex structures to exhibit similar interlamellar spacing regardless of the cationic liposome structures.

The collective transformation of concentric multilamellar structures in LC liposomes into two distinct parts with different interlamellar spacings is a fascinating phenomenon observed in cationic LC-6. In LC-6, the inner regions underwent compaction, while the outer interlamellar spaces expanded with mRNA complexation (Figure S9). This dynamic change disappeared with the excess of mRNA, leading to the anionic LC-0.75 with fingerprint patterns that align with conventional interlamellar spacings. While the direct observation of nucleic acid molecules, such as mRNA, using cryo-EM remains a challenge, their presence can be inferred from their impact on structural features and electron density in lipid assemblies.[76] Specifically, the contrast between the lipid bilayer planes within the lipoplexes was more pronounced than that at their outer edges (see Figure 5). This observation hints at the presence of electron-dense mRNA molecules sandwiched between the lipid membranes, providing a possible explanation for the densely packed multilamellar structures in lipoplexes, as the mRNA molecules can facilitate adhesion between adjacent cationic lipid bilayers.[85] Interestingly, mRNA molecules within the LC-6 exhibited "swelling" distribution in outer lamellae, marked by a wide, high-contrast appearance. This finding aligns with the observed lower ΔGP_{340} values in LC-based lipoplexes (see Figure S3), suggesting a substantial quantity of mRNA is likely confined to this region with a large influx of water, possibly due to the considerable electrostatic interaction with significant presence of cationic DOTAP lipids in the multilamellar bilayers.[86] In contrast, the inner regions of LC-6, with a more compact lamellar structure, appear to accommodate fewer mRNA molecules. This could be attributed to their smaller amounts of cationic lipids and the relative inaccessibility of mRNA within the inner layers of the liposomes. Nonetheless, it is noteworthy that the interlamellar spacing in the inner regions of LC-6 lipoplexes remains larger than that observed in the E400-3 lipoplexes. This suggests that unilamellar lipid membranes in E400 liposomes exhibit a preference for close packing with mRNA, potentially due to their relatively soft nature compared to rigid multilamellar membranes, making them more amenable to transformation.[87,88] On the other hand, the similar interlamellar spacings observed in anionic E400-0.75 and LC-0.75 suggest that a strong electrostatic interaction by excess of mRNA molecules at a very low N/P ratio overcomes the inherent rigidity of multilamellar lipid bilayers, results in the induction of highly packed fingerprint patterns within the lipoplexes.

In summary, the structural comparison reveals intriguing insights into the relationship between the structures of lipid assemblies and the resulting structures of lipoplexes. These findings emphasize that the interplay between cationic liposomes and mRNA complexation is a complex process, and the structure of cationic liposomes significantly impacts the final structure of the mRNA lipoplexes. This knowledge further highlights the critical importance of understanding and manipulating the structural aspects of lipid-based mRNA delivery systems for optimal performance.

CONCLUSIONS

This study systematically explored the biophysical complexities of lipid assemblies in mRNA delivery systems, elucidating the pivotal role of liposome structures in shaping the mRNA lipoplex architecture. Prior to mRNA complexation, cationic DOTAP/DOPE liposomes exhibited notable differences in size distribution and morphology, largely dependent on the fabrication method. Particularly, the LUCA cycle yielded distinctive concentric multilamellar structures in liposomes, which have not been reported in conventional liposomal systems. These structural characteristics in cationic liposomes intimately affected the optimal N/P charge ratio in mRNA lipoplexes, as multilamellar liposomes aggregated at a higher N/P ratio compared to the unilamellar counterparts due to the less exposure of cationic lipids. Furthermore, biological analysis demonstrated that the variability in the optimal N/P ratio within lipoplexes, determined by the structural attributes of cationic liposomes, had a significant impact on biological efficacy. Cryo-EM analysis elucidated the structural differences between lipoplexes, predominantly influenced by the cationic liposome structures and the N/P ratio. Comparative structural analysis of extruded and LUCA-cycled liposomes and lipoplexes further unveiled the preservation of the concentric multilamellar structures in cationic lipoplexes derived from the LUCA-cycled liposome, displaying two distinct interlamellar spacings between inner and outer lamellae. Overall, our findings provide valuable insight into the intricate relationship between the structure of lipid assemblies and the characteristics of the resulting lipoplexes, providing the foundation for the advancement of lipid-based mRNA delivery systems.

https://doi.org/10.1021/acsnano.4c00587
ACS Nano XXXX, XXX, XXX−XXX

MATERIALS AND METHODS

Reagents. 1,2-Dioleoyl-3-trimethylammonium-propane (chloride salt) (DOTAP), 1,2-di(9Z-octadecenoyl)-*sn*-glycero-3-phosphoethanolamine (DOPE), and 1,2-dihexanoyl-*sn*-glycero-3-phosphocholine (DHPC) lipids dissolved in chloroform were obtained from Avanti Polar Lipids (Alabaster, AL). CleanCap Firefly Luciferase mRNA (5 moU) was purchased from TriLink BioTechnologies (San Diego, CA). 6-Dodecanoyl-N,N-dimethyl-2-naphthylamine (Laurdan) was purchased from Sigma-Aldrich (St. Louis, MO).

Mice. BALB/c mice were purchased from InVivos. Mice were accommodated and cared for in a pathogen-free environment, strictly adhering to the institutional protocols established by the Biological Resource Centre (BRC) at A*STAR, Singapore. All procedures involving animals received approval from the Institutional Animal Care and Use Committee (IACUC# 191452).

Liposome Preparation. Liposomes with net positive charge were fabricated by thin-film hydration followed by extrusion or a LUCA cycle. First, the appropriate amounts of long-chain cationic DOTAP, neutral DOPE, and short-chain DHPC lipids in chloroform were added to a glass vial, and the solvent was evaporated by gentle drying under a stream of nitrogen gas and subsequent incubation in a vacuum desiccator overnight. Next, the dried lipid film was hydrated in Milli-Q-treated water (MilliporeSigma, Burlington, MA) or UltraPure DNase/RNase-free distilled water (Thermo Fisher Scientific, Waltham, MA) by vortexing. To prepare E50 and E400 liposomes, the resulting suspensions were extruded using track-etched polycarbonate filter membranes with 50 or 400 nm diameter, respectively. To prepare LC, L4.0, and L2.0 liposomes, the hydrated suspensions were subjected to five LUCA cycles, involving the following steps: (1) submerse in liquid nitrogen for 1 min, (2) thaw in a 60 °C water bath for 5 min, and (3) vortex for 30 s. The DOTAP and DOPE concentrations were fixed at 10 mM unless stated otherwise.

Lipoplex Preparation. Lipoplex formation was performed based on the protocols described previously with slight modifications.[40,89] A diversity of formulations complexed with the reporter firefly luciferase (Luc)-encoding mRNA was assembled with cationic liposomes to create various N/P ratios, which defined the charge ratio and overall lipoplex net charge. The charge ratios were calculated from the molar ratio of positively charged amine (N = nitrogen) groups to negatively charged phosphate (P) groups, represented by mRNA nucleotides. For the calculation of the molar ratio between the cationic lipid and mRNA, a mean molar mass of 330 Da per nucleotide was assumed. mRNA was provided as a sodium citrate-buffered solution at an mRNA concentration of 1 mg/mL. Lipoplexes were formed by diluting the mRNA with UltraPure DNase/RNase-free distilled water followed by adding an appropriate amount of cationic liposome dispersion to reach the selected charge ratio.

DLS and Zeta Potential Measurements. The size distribution and zeta potential were investigated by using a 90Plus particle size/zeta PALS analyzer (Brookhaven Instruments Corporation, NY). For size distribution analysis, measurements were based on DLS at a scattering angle of 90° to minimize the reflection effect. All autocorrelation functions obtained were analyzed by the cumulant method and fitted to multimodal distribution(s) to obtain size distributions.

Generalized Polarization Measurement. Ten millimolars of 0.5 mol % Laurdan-labeled liposomes were diluted to a total lipid concentration of 0.5 mM with UltraPure DNase/RNase-free distilled water. Lipoplexes were formed with 0.5 mol % Laurdan-labeled cationic liposomes and diluted five times with UltraPure DNase/RNase-free distilled water. Laurdan fluorescence was measured by scanning emission wavelengths between 420 and 520 nm with an excitation wavelength of 340 nm. Generalized polarization (GP) with an excitation wavelength of 340 nm (GP_{340}) was calculated as follows:

$$GP_{340} = \frac{(I_{440} - I_{490})}{(I_{440} + I_{490})}$$

wherein I_{440} and I_{490} are the emission intensities at wavelengths of 440 and 490 nm, respectively. A higher GP_{340} value represents a lower hydration level (dehydration) on the liposomal surface.[61]

Cryogenic Electron Microscopy (Cryo-EM). To prepare samples for cryo-EM imaging, lacey carbon−coated 300 mesh copper grids (Electron Microscopy Sciences, Hatfield, PA) were glow discharged. Four microliters of sample solution was deposited onto a grid at 100% humidity, blotted with filter paper (2 s blotting time, 0 blot force), and plunged into liquid ethane (Vitrobot, FEI Company). Cryo-grids were imaged by using a FEG 200 keV transmission electron microscope (Arctica, FEI Company) equipped with a direct electron detector (Falcon II, FEI Company). Images were recorded at a nominal 53,000× magnification with an integration time (exposure time) of 1 s. FFT of cryo-EM images were obtained with ImageJ software. The analysis of liposome morphology was conducted manually with each population comprising a minimum of 80 particles. To ensure precise categorization and eliminate the influence of structural abnormalities caused by sample preparation or variations in ice thickness, only unobstructed liposomes with clearly defined edges were included in the quantitative structural analysis.

***In Vitro* Luciferase Transfection Assay.** HEK293T cell lines (ATCC, Manassas, VA) were cultured in Dulbecco's modified Eagle's medium (Gibco) supplemented with 10% heat-inactivated fetal bovine serum (Gibco) and 1% penicillin/streptomycin (Hyclone). All cultures were grown in 37 °C incubators supplemented with 5% CO_2 and maintained following suppliers' instructions. For assays, cells were seeded onto 96-well plates at a density of 5000 cells per well and allowed to adhere overnight. Then, mRNA lipoplexes were added to the cell media in which the cells are cultured with 100 and 200 ng of mRNA per well. Luciferase expression data were collected after 24-h post-treatment with a microplate reader using Pierce Firefly Luciferase Glow Assay Kit (Thermo Fisher Scientific, Waltham, MA) by following suppliers' instructions and normalized by the expression level of E400-3 with 100 ng.

Cell Viability Assay. Cell viability was evaluated using the Cell Counting Kit-8 (CCK-8, Dojindo) assay. Briefly, HEK293T cells were treated with mRNA lipoplexes with 100 and 200 ng of mRNA per well. After 24 h of incubation, the cells were washed with DPBS and CCK-8 solution was added to each well followed by incubation for 2 h. Cell viability data were collected by measuring the absorbance at 450 nm with a microplate reader.

***In Vivo* Bioluminescence Imaging.** 5−8 weeks male BALB/c mice were intravenously (i.v.) injected with 10 μg of FLuc mRNA complexed with lipoplexes through the lateral tail veins. Six hours after the lipoplex administration, the mice were injected with 150 mg/kg of D-luciferin (Thermo Fisher Scientific, Waltham, MA) dissolved in PBS through intraperitoneal injection, and thereafter given 10 min allowance for the complete systemic circulation of luciferin, before performing *in vivo* bioluminescence imaging. After 24 h, mice were reinjected with 150 mg/kg of D-luciferin in PBS, with a 10 min pause, before the livers, lungs, and spleens were harvested and imaged for bioluminescence. Bioluminescence image acquisition was performed using the IVIS Spectrum In Vivo Imaging System (PerkinElmer, Shelton, CT). All image postprocessing and analyses were performed using the Living Image 4.8.0 software (PerkinElmer, Shelton, CT). Bioluminescence intensities were quantified by drawing respective regions of interest (ROI) around the livers, lungs, and spleens and measuring the radiance within each ROI.

ASSOCIATED CONTENT

Supporting Information

The Supporting Information is available free of charge at https://pubs.acs.org/doi/10.1021/acsnano.4c00587.

Table for average diameters, PDI, and zeta potential values for cationic liposomes, cryo-EM images for L0.5, GP_{340} values of Laurdan in cationic liposomes, effect of N/P ratio on the GP_{340} values of Laurdan in E400- and LC-based lipoplexes, *in vitro* transfection efficiency of

https://doi.org/10.1021/acsnano.4c00587
ACS Nano XXXX, XXX, XXX−XXX

VOR and E50-based lipoplexes at varied N/P charge ratio of respective cationic liposomes, stability analysis of E400- and LC-based lipoplexes freshly constituted or stored at 4 °C for 1 week after constitution, cell viability of E400- and LC-based lipoplexes, bioluminescence imaging of BALB/c mice after IV administration of cationic E400-6, representative FFT, and pixel intensity profile analysis for comparison of self-assembly structures between E400 and LC-based lipoplexes, and comparison of the interlamellar spacing of LC and LC-based lipoplexes analyzed using the pixel intensity profile from cryo-EM images (PDF)

AUTHOR INFORMATION

Corresponding Authors

Sangyong Jung − *Institute of Molecular and Cell Biology (IMCB), Agency for Science, Technology and Research (A*STAR), Singapore 138673, Singapore; Department of Medical Science, College of Medicine, CHA University, Seongnam 13488, Republic of Korea*; Email: jungsy0505@cha.ac.kr

Nam-Joon Cho − *School of Materials Science and Engineering, Nanyang Technological University, Singapore 639798, Singapore*; orcid.org/0000-0002-8692-8955; Email: njcho@ntu.edu.sg

Authors

Hyunhyuk Tae − *School of Materials Science and Engineering, Nanyang Technological University, Singapore 639798, Singapore*; orcid.org/0000-0002-0459-5879

Soohyun Park − *School of Materials Science and Engineering, Nanyang Technological University, Singapore 639798, Singapore*; orcid.org/0000-0003-3261-7585

Li Yang Tan − *Institute of Molecular and Cell Biology (IMCB), Agency for Science, Technology and Research (A*STAR), Singapore 138673, Singapore; Department of Psychological Medicine, Yong Loo Lin School of Medicine, National University of Singapore, Singapore 119228, Singapore*

Chungmo Yang − *School of Materials Science and Engineering, Nanyang Technological University, Singapore 639798, Singapore*

Yong-An Lee − *Genome Institute of Singapore (GIS), Agency for Science, Technology and Research (A*STAR), Singapore 138672, Singapore*

Younghwan Choe − *School of Materials Science and Engineering, Nanyang Technological University, Singapore 639798, Singapore*

Torsten Wüstefeld − *Lee Kong Chian School of Medicine and School of Biological Science, Nanyang Technological University, Singapore 637551, Singapore; Genome Institute of Singapore (GIS), Agency for Science, Technology and Research (A*STAR), Singapore 138672, Singapore*

Complete contact information is available at: https://pubs.acs.org/10.1021/acsnano.4c00587

Author Contributions

○H.T. and S.P. contributed equally to this work.

Notes

The authors declare no competing financial interest.

ACKNOWLEDGMENTS

We would like to acknowledge the Facility for Analysis, Characterization, Testing and Simulation, Nanyang Technological University, Singapore, for the use of their cryo-EM and thank Dr. P.J.S.B. for the SAXS experiments. In addition, we thank valuable technical discussion with Dr. J.A.J. This research was supported by the Ministry of Education (MOE) in Singapore under grants RG111/20, RG34/22 and MOE-MOET32022-0002, and by a sponsored research agreement from LUCA AICell Inc. (RCA-LUCA AICell REQ0239282). In addition, this work was supported by National Research Foundation in Singapore (NRF) under grant REQ414940. This work was also supported by National Research Foundation of Korea (NRF) grants funded by the Ministry of Science and ICT (2021K1A4A7A0209781012) and National Institute of Health (NIH) grants funded by the Korea Disease Control and Prevention Agency (KDCA) (2022ER240600). H.T. was supported by a SINGA graduate scholarship from the A*STAR Graduate Academy, Singapore. The LUCA cycle is a proprietary technology developed by LUCA AICell Inc., with T.H. Kim being the credited inventor of this advanced processing method, for which a TD has been filed.

REFERENCES

(1) Liu, Y.; Miyoshi, H.; Nakamura, M. Nanomedicine for drug delivery and imaging: a promising avenue for cancer therapy and diagnosis using targeted functional nanoparticles. *Int. J. Cancer.* **2007**, *120* (12), 2527−2537.

(2) Kumar, R.; Santa Chalarca, C. F.; Bockman, M. R.; Bruggen, C. V.; Grimme, C. J.; Dalal, R. J.; Hanson, M. G.; Hexum, J. K.; Reineke, T. M. Polymeric delivery of therapeutic nucleic acids. *Chem. Rev.* **2021**, *121* (18), 11527−11652.

(3) Tan, X.; Jia, F.; Wang, P.; Zhang, K. Nucleic acid-based drug delivery strategies. *J. Controlled Release* **2020**, *323*, 240−252.

(4) Hou, X.; Zaks, T.; Langer, R.; Dong, Y. Lipid nanoparticles for mRNA delivery. *Nat. Rev. Mater.* **2021**, *6* (12), 1078−1094.

(5) Ferhan, A. R.; Park, S.; Park, H.; Tae, H.; Jackman, J. A.; Cho, N. J. Lipid nanoparticle technologies for nucleic acid delivery: A nanoarchitectonics perspective. *Adv. Funct. Mater.* **2022**, *32* (37), No. 2203669.

(6) Labouta, H. I.; Langer, R.; Cullis, P. R.; Merkel, O. M.; Prausnitz, M. R.; Gomaa, Y.; Nogueira, S. S.; Kumeria, T. Role of drug delivery technologies in the success of COVID-19 vaccines: a perspective. *Drug Delivery Transl. Res.* **2022**, *12* (11), 2581−2588.

(7) Kauffman, K. J.; Dorkin, J. R.; Yang, J. H.; Heartlein, M. W.; DeRosa, F.; Mir, F. F.; Fenton, O. S.; Anderson, D. G. Optimization of lipid nanoparticle formulations for mRNA delivery in vivo with fractional factorial and definitive screening designs. *Nano Lett.* **2015**, *15* (11), 7300−7306.

(8) Wang, C.; Zhang, Y.; Dong, Y. Lipid Nanoparticle−mRNA Formulations for Therapeutic Applications. *Acc. Chem. Res.* **2021**, *54* (23), 4283−4293.

(9) Zheng, L.; Bandara, S. R.; Tan, Z.; Leal, C. Lipid nanoparticle topology regulates endosomal escape and delivery of RNA to the cytoplasm. *Proc. Natl. Acad. Sci. U. S. A.* **2023**, *120* (27), No. e2301067120.

(10) Felgner, J. H.; Kumar, R.; Sridhar, C.; Wheeler, C. J.; Tsai, Y. J.; Border, R.; Ramsey, P.; Martin, M.; Felgner, P. L. Enhanced gene delivery and mechanism studies with a novel series of cationic lipid formulations. *J. Biol. Chem.* **1994**, *269* (4), 2550−2561.

(11) Simberg, D.; Danino, D.; Talmon, Y.; Minsky, A.; Ferrari, M. E.; Wheeler, C. J.; Barenholz, Y. Phase behavior, DNA ordering, and size instability of cationic lipoplexes: relevance to optimal transfection activity. *J. Biol. Chem.* **2001**, *276* (50), 47453−47459.

(12) Koltover, I.; Salditt, T.; Rädler, J. O.; Safinya, C. R. An inverted hexagonal phase of cationic liposome-DNA complexes related to DNA release and delivery. *Science* **1998**, *281* (5373), 78−81.
(13) Settanni, G.; Brill, W.; Haas, H.; Schmid, F. pH-Dependent Behavior of Ionizable Cationic Lipids in mRNA-Carrying Lipoplexes Investigated by Molecular Dynamics Simulations. *Macromol. Rapid Commun.* **2022**, *43* (12), No. 2100683.
(14) Habrant, D.; Peuziat, P.; Colombani, T.; Dallet, L.; Gehin, J.; Goudeau, E.; Evrard, B.; Lambert, O.; Haudebourg, T.; Pitard, B. Design of ionizable lipids to overcome the limiting step of endosomal escape: application in the intracellular delivery of mRNA, DNA, and siRNA. *J. Med. Chem.* **2016**, *59* (7), 3046−3062.
(15) Cheng, Q.; Wei, T.; Farbiak, L.; Johnson, L. T.; Dilliard, S. A.; Siegwart, D. J. Selective organ targeting (SORT) nanoparticles for tissue-specific mRNA delivery and CRISPR−Cas gene editing. *Nat. Nanotechnol.* **2020**, *15* (4), 313−320.
(16) Hassett, K. J.; Higgins, J.; Woods, A.; Levy, B.; Xia, Y.; Hsiao, C. J.; Acosta, E.; Almarsson, Ö.; Moore, M. J.; Brito, L. A. Impact of lipid nanoparticle size on mRNA vaccine immunogenicity. *J. Controlled Release* **2021**, *335*, 237−246.
(17) Tranchant, I.; Thompson, B.; Nicolazzi, C.; Mignet, N.; Scherman, D. Physicochemical optimization of plasmid delivery by cationic lipids. *J. Gene Med.* **2004**, *6* (S1), S24−S35.
(18) Yang, S.; Chen, J.; Zhao, D.; Han, D.; Chen, X. Comparative study on preparative methods of DC-Chol/DOPE liposomes and formulation optimization by determining encapsulation efficiency. *Int. J. Pharm.* **2012**, *434* (1−2), 155−160.
(19) Meisel, J. W.; Gokel, G. W. A simplified direct lipid mixing lipoplex preparation: Comparison of liposomal-, dimethylsulfoxide-, and ethanol-based methods. *Sci. Rep.* **2016**, *6* (1), No. 27662.
(20) Maitani, Y.; Igarashi, S.; Sato, M.; Hattori, Y. Cationic liposome (DC-Chol/DOPE= 1:2) and a modified ethanol injection method to prepare liposomes, increased gene expression. *Int. J. Pharm.* **2007**, *342* (1−2), 33−39.
(21) Ross, P.; Hui, S. Lipoplex size is a major determinant of in vitro lipofection efficiency. *Gene Ther.* **1999**, *6* (4), 651−659.
(22) Almofti, M. R.; Harashima, H.; Shinohara, Y.; Almofti, A.; Li, W.; Kiwada, H. Lipoplex size determines lipofection efficiency with or without serum. *Mol. Membr. Biol.* **2003**, *20* (1), 35−43.
(23) Ramezani, M.; Khoshhamdam, M.; Dehshahri, A.; Malaekeh-Nikouei, B. The influence of size, lipid composition and bilayer fluidity of cationic liposomes on the transfection efficiency of nanolipoplexes. *Colloids Surf. B: Biointerfaces* **2009**, *72* (1), 1−5.
(24) Bruininks, B. M.; Souza, P. C.; Ingolfsson, H.; Marrink, S. J. A molecular view on the escape of lipoplexed DNA from the endosome. *Elife* **2020**, *9*, No. e52012.
(25) Lapinski, M. M.; Castro-Forero, A.; Greiner, A. J.; Ofoli, R. Y.; Blanchard, G. J. Comparison of liposomes formed by sonication and extrusion: rotational and translational diffusion of an embedded chromophore. *Langmuir* **2007**, *23* (23), 11677−11683.
(26) Çağdaş, M.; Sezer, A. D.; Bucak, S. Liposomes as potential drug carrier systems for drug delivery. In *Application of nanotechnology in drug delivery 2*; Sezer, A. D., Ed.; InTech: Croatia, 2014; pp 1−50.
(27) Costa, A. P.; Xu, X.; Burgess, D. J. Freeze-anneal-thaw cycling of unilamellar liposomes: effect on encapsulation efficiency. *Pharm. Res.* **2014**, *31*, 97−103.
(28) Sriwongsitanont, S.; Ueno, M. Effect of freeze-thawing process on the size and lamellarity of peg-lipid liposomes. *Open Colloid Sci. J.* **2010**, *4*, 1.
(29) MacDonald, R. C.; Jones, F. D.; Qui, R. Fragmentation into small vesicles of dioleoylphosphatidylcholine bilayers during freezing and thawing. *Biochim. Biophys. Acta. Biomembr.* **1994**, *1191* (2), 362−370.
(30) Traïkia, M.; Warschawski, D. E.; Recouvreur, M.; Cartaud, J.; Devaux, P. F. Formation of unilamellar vesicles by repetitive freeze-thaw cycles: characterization by electron microscopy and 31 P-nuclear magnetic resonance. *Eur. Biophys. J.* **2000**, *29*, 184−195.
(31) Sut, T. N.; Park, S.; Choe, Y.; Cho, N.-J. Characterizing the supported lipid membrane formation from cholesterol-rich bicelles. *Langmuir* **2019**, *35* (47), 15063−15070.
(32) Sut, T. N.; Jackman, J. A.; Yoon, B. K.; Park, S.; Kolahdouzan, K.; Ma, G. J.; Zhdanov, V. P.; Cho, N.-J. Influence of NaCl concentration on bicelle-mediated SLB formation. *Langmuir* **2019**, *35* (32), 10658−10666.
(33) Zelphati, O.; Nguyen, C.; Ferrari, M.; Felgner, J.; Tsai, Y.; Felgner, P. Stable and monodisperse lipoplex formulations for gene delivery. *Gene Ther.* **1998**, *5* (9), 1272−1282.
(34) Wasungu, L.; Hoekstra, D. Cationic lipids, lipoplexes and intracellular delivery of genes. *J. Controlled Release* **2006**, *116* (2), 255−264.
(35) Pitard, B.; Oudrhiri, N.; Vigneron, J.-P.; Hauchecorne, M.; Aguerre, O.; Toury, R.; Airiau, M.; Ramasawmy, R.; Scherman, D.; Crouzet, J. Structural characteristics of supramolecular assemblies formed by guanidinium-cholesterol reagents for gene transfection. *Proc. Natl. Acad. Sci. U. S. A.* **1999**, *96* (6), 2621−2626.
(36) Kennedy, M. T.; Pozharski, E. V.; Rakhmanova, V. A.; MacDonald, R. C. Factors governing the assembly of cationic phospholipid-DNA complexes. *Biophys. J.* **2000**, *78* (3), 1620−1633.
(37) Elizondo, E.; Moreno, E.; Cabrera, I.; Córdoba, A.; Sala, S.; Veciana, J.; Ventosa, N. Liposomes and other vesicular systems: structural characteristics, methods of preparation, and use in nanomedicine. *Prog. Mol. Biol. Transl. Sci.* **2011**, *104*, 1−52.
(38) Rädler, J. O.; Koltover, I.; Salditt, T.; Safinya, C. R. Structure of DNA-cationic liposome complexes: DNA intercalation in multilamellar membranes in distinct interhelical packing regimes. *Science* **1997**, *275* (5301), 810−814.
(39) Kim, B.-K.; Hwang, G.-B.; Seu, Y.-B.; Choi, J.-S.; Jin, K. S.; Doh, K.-O. DOTAP/DOPE ratio and cell type determine transfection efficiency with DOTAP-liposomes. *Biochim. Biophys. Acta. Biomembr.* **2015**, *1848* (10), 1996−2001.
(40) Kranz, L. M.; Diken, M.; Haas, H.; Kreiter, S.; Loquai, C.; Reuter, K. C.; Meng, M.; Fritz, D.; Vascotto, F.; Hefesha, H. Systemic RNA delivery to dendritic cells exploits antiviral defence for cancer immunotherapy. *Nature* **2016**, *534* (7607), 396−401.
(41) Grabbe, S.; Haas, H.; Diken, M.; Kranz, L. M.; Langguth, P.; Sahin, U. Translating nanoparticulate-personalized cancer vaccines into clinical applications: case study with RNA-lipoplexes for the treatment of melanoma. *Nanomedicine* **2016**, *11* (20), 2723−2734.
(42) Safinya, C. R. Structures of lipid−DNA complexes: supramolecular assembly and gene delivery. *Curr. Opin. Struct. Biol.* **2001**, *11* (4), 440−448.
(43) Felgner, P. L.; Gadek, T. R.; Holm, M.; Roman, R.; Chan, H. W.; Wenz, M.; Northrop, J. P.; Ringold, G. M.; Danielsen, M. Lipofection: a highly efficient, lipid-mediated DNA-transfection procedure. *Prog. Mol. Biol. Transl. Sci.* **1987**, *84* (21), 7413−7417.
(44) Sanders, C. R.; Schwonek, J. P. Characterization of magnetically orientable bilayers in mixtures of dihexanoylphosphatidylcholine and dimyristoylphosphatidylcholine by solid-state NMR. *Biochemistry* **1992**, *31* (37), 8898−8905.
(45) Dürr, U. H.; Soong, R.; Ramamoorthy, A. When detergent meets bilayer: birth and coming of age of lipid bicelles. *Prog. Nucl. Magn. Reson. Spectrosc.* **2013**, *69*, 1.
(46) Rodriguez, G.; Cocera, M.; Rubio, L.; Lopez-Iglesias, C.; Pons, R.; de la Maza, A.; Lopez, O. A unique bicellar nanosystem combining two effects on stratum corneum lipids. *Mol. Pharmaceutics.* **2012**, *9* (3), 482−491.
(47) Rodríguez, G.; Rubio, L.; Barba, C.; López-Iglesias, C.; de la Maza, A.; López, O.; Cócera, M. Characterization of new DOPC/DHPC platform for dermal applications. *Eur. Biophys. J.* **2013**, *42*, 333−345.
(48) Choi, S.; Kang, B.; Yang, E.; Kim, K.; Kwak, M. K.; Chang, P.-S.; Jung, H.-S. Precise control of liposome size using characteristic time depends on solvent type and membrane properties. *Sci. Rep.* **2023**, *13* (1), 4728.
(49) Harroun, T. A.; Koslowsky, M.; Nieh, M.-P.; de Lannoy, C.-F.; Raghunathan, V.; Katsaras, J. Comprehensive examination of

https://doi.org/10.1021/acsnano.4c00587
ACS Nano XXXX, XXX, XXX−XXX

mesophases formed by DMPC and DHPC mixtures. *Langmuir* **2005**, *21* (12), 5356−5361.
(50) Bangham, A. Properties and uses of lipid vesicles: an overview. *Ann. N.Y. Acad. Sci.* **1978**, *308* (1), 2−7.
(51) Jackman, J. A.; Cho, N.-J. Supported lipid bilayer formation: beyond vesicle fusion. *Langmuir* **2020**, *36* (6), 1387−1400.
(52) Crauste-Manciet, S.; Larquet, E.; Khawand, K.; Bessodes, M.; Chabot, G. G.; Brossard, D.; Mignet, N. Lipidic spherulites: Formulation optimization by paired optical and cryoelectron microscopy. *Eur. J. Pharm. Biopharm.* **2013**, *85* (3), 1088−1094.
(53) Gulik-Krzywicki, T.; Dedieu, J.; Roux, D.; Degert, C.; Laversanne, R. Freeze−Fracture Electron Microscopy of Sheared Lamellar Phase. *Langmuir* **1996**, *12* (20), 4668−4671.
(54) Zhang, Y.; Zhou, G.; Sun, B.; Zhao, M.; Zhang, J.; Chen, F. A cationic−cationic co-surfactant templating route for synthesizing well-defined multilamellar vesicular silica with an adjustable number of layers. *Chem. Commun.* **2014**, *50* (22), 2907−2909.
(55) Monnard, P.-A.; Oberholzer, T.; Luisi, P. Entrapment of nucleic acids in liposomes. *Biochim. Biophys. Acta. Biomembr* **1997**, *1329* (1), 39−50.
(56) Laouini, A.; Jaafar-Maalej, C.; Limayem-Blouza, I.; Sfar, S.; Charcosset, C.; Fessi, H. Preparation, characterization and applications of liposomes: state of the art. *J. Colloid Sci. Biotechnol.* **2012**, *1* (2), 147−168.
(57) Tenchov, R.; Bird, R.; Curtze, A. E.; Zhou, Q. Lipid nanoparticles— from liposomes to mRNA vaccine delivery, a landscape of research diversity and advancement. *ACS Nano* **2021**, *15* (11), 16982−17015.
(58) Kolahdouzan, K.; Jackman, J. A.; Yoon, B. K.; Kim, M. C.; Johal, M. S.; Cho, N.-J. Optimizing the formation of supported lipid bilayers from bicellar mixtures. *Langmuir* **2017**, *33* (20), 5052−5064.
(59) Harris, F. M.; Best, K. B.; Bell, J. D. Use of laurdan fluorescence intensity and polarization to distinguish between changes in membrane fluidity and phospholipid order. *Biochim. Biophys. Acta. Biomembr* **2002**, *1565* (1), 123−128.
(60) Zhang, Y.-L.; Frangos, J. A.; Chachisvilis, M. Laurdan fluorescence senses mechanical strain in the lipid bilayer membrane. *Biochem. Biophys. Res. Commun.* **2006**, *347* (3), 838−841.
(61) Maitani, Y.; Nakamura, A.; Tanaka, T.; Aso, Y. Hydration of surfactant-modified and PEGylated cationic cholesterol-based liposomes and corresponding lipoplexes by monitoring a fluorescent probe and the dielectric relaxation time. *Int. J. Pharm.* **2012**, *427* (2), 372−378.
(62) Hirsch-Lerner, D.; Barenholz, Y. Hydration of lipoplexes commonly used in gene delivery: follow-up by laurdan fluorescence changes and quantification by differential scanning calorimetry. *Biochim. Biophys. Acta. Biomembr* **1999**, *1461* (1), 47−57.
(63) Risselada, H. J.; Marrink, S. J. Curvature effects on lipid packing and dynamics in liposomes revealed by coarse grained molecular dynamics simulations. *Phys. Chem. Chem. Phys.* **2009**, *11* (12), 2056−2067.
(64) Semenova, A.; Chugunov, A.; Dubovskii, P.; Chupin, V.; Volynsky, P.; Boldyrev, I. The role of chain rigidity in lipid self-association: Comparative study of dihexanoyl-and disorbyl-phosphatidylcholines. *Chem. Phys. Lipids.* **2012**, *165* (4), 382−386.
(65) Birchall, J. C.; Kellaway, I. W.; Mills, S. N. Physico-chemical characterisation and transfection efficiency of lipid-based gene delivery complexes. *Int. J. Pharm.* **1999**, *183* (2), 195−207.
(66) Zuidam, N. J.; Barenholz, Y. Electrostatic and structural properties of complexes involving plasmid DNA and cationic lipids commonly used for gene delivery. *Biochim. Biophys. Acta. Biomembr* **1998**, *1368* (1), 115−128.
(67) Klein, E.; Ciobanu, M.; Klein, J.; Machi, V.; Leborgne, C.; Vandamme, T.; Frisch, B. T.; Pons, F.; Kichler, A.; Zuber, G. HFP" fluorinated cationic lipids for enhanced lipoplex stability and gene delivery. *Bioconjugate Chem.* **2010**, *21* (2), 360−371.
(68) Masotti, A.; Mossa, G.; Cametti, C.; Ortaggi, G.; Bianco, A.; Del Grosso, N.; Malizia, D.; Esposito, C. Comparison of different commercially available cationic liposome−DNA lipoplexes: Parameters influencing toxicity and transfection efficiency. *Colloids Surf., B* **2009**, *68* (2), 136−144.
(69) Han, X.; Gong, N.; Xue, L.; Billingsley, M. M.; El-Mayta, R.; Shepherd, S. J.; Alameh, M.-G.; Weissman, D.; Mitchell, M. J. Ligand-tethered lipid nanoparticles for targeted RNA delivery to treat liver fibrosis. *Nat. Commun.* **2023**, *14* (1), 75.
(70) Ewert, K.; Slack, N. L.; Ahmad, A.; Evans, H. M.; Lin, A. J.; Samuel, C. E.; Safinya, C. R. Cationic lipid-DNA complexes for gene therapy: understanding the relationship between complex structure and gene delivery pathways at the molecular level. *Curr. Med. Chem.* **2004**, *11* (2), 133−149.
(71) Bandara, S. R.; Molley, T. G.; Kim, H.; Bharath, P. A.; Kilian, K. A.; Leal, C. The structural fate of lipid nanoparticles in the extracellular matrix. *Mater. Horiz.* **2020**, *7* (1), 125−134.
(72) Eygeris, Y.; Patel, S.; Jozic, A.; Sahay, G. Deconvoluting lipid nanoparticle structure for messenger RNA delivery. *Nano Lett.* **2020**, *20* (6), 4543−4549.
(73) Bernasconi, V.; Norling, K.; Bally, M.; Höök, F.; Lycke, N. Y. Mucosal vaccine development based on liposome technology. *J. Immunol. Res.* **2016**, *2016*, No. 5482087, DOI: 10.1155/2016/5482087.
(74) Patel, G. B.; Zhou, H.; Ponce, A.; Chen, W. Mucosal and systemic immune responses by intranasal immunization using archaeal lipid-adjuvanted vaccines. *Vaccine* **2007**, *25* (51), 8622−8636.
(75) Rodriguez-Pulido, A.; Martin-Molina, A.; Rodriguez-Beas, C.; Llorca, O.; Aicart, E.; Junquera, E. A theoretical and experimental approach to the compaction process of DNA by dioctadecyldimethylammonium bromide/zwitterionic mixed liposomes. *J. Phys. Chem. B* **2009**, *113* (47), 15648−15661.
(76) Weisman, S.; Hirsch-Lerner, D.; Barenholz, Y.; Talmon, Y. Nanostructure of cationic lipid-oligonucleotide complexes. *Biophys. J.* **2004**, *87* (1), 609−614.
(77) Xu, Y.; Hui, S.-W.; Frederik, P.; Szoka, F. C. Physicochemical characterization and purification of cationic lipoplexes. *Biophys. J.* **1999**, *77* (1), 341−353.
(78) Sternberg, B.; Sorgi, F. L.; Huang, L. New structures in complex formation between DNA and cationic liposomes visualized by freeze—fracture electron microscopy. *FEBS Lett.* **1994**, *356* (2−3), 361−366.
(79) Farge, E.; Devaux, P. F. Size-dependent response of liposomes to phospholipid transmembrane redistribution: from shape change to induced tension. *J. Phys. Chem.* **1993**, *97* (12), 2958−2961.
(80) Mitrea, D. M.; Chandra, B.; Ferrolino, M. C.; Gibbs, E. B.; Tolbert, M.; White, M. R.; Kriwacki, R. W. Methods for physical characterization of phase-separated bodies and membrane-less organelles. *J. Mol. Biol.* **2018**, *430* (23), 4773−4805.
(81) Dittrich, M.; Brauer, C.; Funari, S. S.; Dobner, B.; Brezesinski, G.; Wölk, C. Interactions of cationic lipids with DNA: A structural approach. *Langmuir* **2018**, *34* (49), 14858−14868.
(82) Martínez-Negro, M.; Guerrero-Martínez, A. S.; García-Río, L.; Domènech, O. S.; Aicart, E.; Tros de Ilarduya, C.; Junquera, E. Multidisciplinary approach to the transfection of plasmid DNA by a nonviral nanocarrier based on a gemini−bolaamphiphilic hybrid lipid. *ACS omega* **2018**, *3* (1), 208−217.
(83) Kumar, K.; Barrán-Berdón, A. L.; Datta, S.; Muñoz-Úbeda, M.; Aicart-Ramos, C.; Kondaiah, P.; Junquera, E.; Bhattacharya, S.; Aicart, E. A delocalizable cationic headgroup together with an oligo-oxyethylene spacer in gemini cationic lipids improves their biological activity as vectors of plasmid DNA. *J. Mater. Chem. B* **2015**, *3* (8), 1495−1506.
(84) Koynova, R.; MacDonald, R. C. Columnar DNA superlattices in lamellar o-ethylphosphatidylcholine lipoplexes: mechanism of the gel-liquid crystalline lipid phase transition. *Nano Lett.* **2004**, *4* (8), 1475−1479.
(85) Uebbing, L.; Ziller, A.; Siewert, C.; Schroer, M. A.; Blanchet, C. E.; Svergun, D. I.; Ramishetti, S.; Peer, D.; Sahin, U.; Haas, H. Investigation of pH-responsiveness inside lipid nanoparticles for parenteral mRNA application using small-angle X-ray scattering. *Langmuir* **2020**, *36* (44), 13331−13341.

https://doi.org/10.1021/acsnano.4c00587
ACS Nano XXXX, XXX, XXX−XXX

(86) Ziller, A.; Nogueira, S. S.; Hühn, E.; Funari, S. S.; Brezesinski, G.; Hartmann, H.; Sahin, U.; Haas, H.; Langguth, P. Incorporation of mRNA in lamellar lipid matrices for parenteral administration. *Mol. Pharmaceutics* **2018**, *15* (2), 642−651.
(87) Sagar, G. H.; Bellare, J. R. Estimation of mechanical strength of unilamellar and multilamellar AOT/Water vesicles and their rupture using micropipet aspiration. *J. Phys. Chem. B* **2009**, *113* (42), 13805−13810.
(88) De Haas, K.; Blom, C.; Van den Ende, D.; Duits, M. H.; Mellema, J. Deformation of giant lipid bilayer vesicles in shear flow. *Phys. Rev. E* **1997**, *56* (6), 7132.
(89) Barichello, J. M.; Ishida, T.; Kiwada, H., Complexation of siRNA and pDNA with cationic liposomes: the important aspects in lipoplex preparation. In *Liposomes: Methods and Protocols, Vol. 1: Pharmaceutical Nanocarriers*; Weissig, V., Ed.; Humana Press, 2010; pp 461−472.

https://doi.org/10.1021/acsnano.4c00587
ACS Nano XXXX, XXX, XXX−XXX